Faraday Discussions

Cite this: *Faraday Discuss.*, 2025, **259**, 149

ROYAL SOCIETY OF CHEMISTRY

PAPER

View Article Online
View Journal | View Issue

Fabrication and characterization of phosphoinositide containing asymmetric vesicles in physiological salt

Trevor A. Paratore, Alonzo H. Ross and Arne Gericke *

Received 9th December 2024, Accepted 30th January 2025
DOI: 10.1039/d4fd00191e

Phosphoinositide (PIPs) lipids mediate a broad range of physiological functions by attracting proteins at specific time points to distinct cellular sites. Many of these processes are associated with the local accumulation of PIPs and PIP/protein signaling platform formation. Studies aimed at determining the physicochemical underpinnings of PIP domain formation have been limited to model systems that exhibited the same lipid composition in both bilayer leaflets. However, biological membranes are asymmetric, and it is desirable to develop an experimental approach that allows for the fabrication of lipid model systems with a non-symmetric lipid bilayer, *i.e.*, a membrane mimic that exhibits a PIP containing lipid mixture in one leaflet and a different lipid composition in the opposing leaflet. We adapted the previously introduced hemifusion method for the fabrication of asymmetric Giant Unilamellar Vesicles (aGUVs) for the fabrication of aGUVs with phosphatidylinositol-(4,5)-bisphosphate ($PI(4,5)P_2$) in a physiological ionic strength buffer solution. The general method involved the bivalent cation-initiated fusion of a symmetric GUV (sGUV) with solid-supported lipid bilayers, which leads to the exchange of the outer leaflet of the sGUV. We find that initiating the hemifusion with 6 mM Ca^{2+} leads to a low yield and quality of the aGUVs. We attribute this to macroscopic $Ca^{2+}/PI(4,5)P_2$ domain formation of the solid support lipid bilayer (SLB), which leads to the interaction of the sGUVs with regions enriched in $PI(4,5)P_2$ (domain) and other areas that are void of the PIP lipid. Using 6 mM Mg^{2+} as the initiator instead led to an improvement in terms of yield and aGUV quality. The best results were obtained when using 1 mM Mg^{2+}. We are introducing several data analysis approaches that allow for the identification of aGUVs that exhibit high quality in terms of the outer leaflet exchange and composition of the two aGUV leaflets.

1 Introduction

Phosphoinositides (PIPs) are anionic phospholipids that mediate a broad range of cellular functions by attracting proteins to specific cellular sites at specific

Worcester Polytechnic Institute, Department of Chemistry and Biochemistry, 100 Institute Rd, Worcester, MA, 01609, USA. E-mail: agericke@wpi.edu; Tel: +1-5088315263

times. It has been shown for certain PIP moieties that the level of protein mediation they accomplish is associated with their enrichment in particular areas of the cell.[1,2] Such areas of enrichment, or domains, are distinct in their lipid and protein composition and provide an environment conducive to the signaling event taking place. Other examples of phosphoinositide distributions are the generation of PIP gradients during cell migration or the non-uniform distribution of phosphoinositides in polarized cells (*e.g.* epithelial cells).[3,4]

Biological membranes generally exhibit lateral and vertical asymmetry. Lateral asymmetry can manifest in the form of heterogeneous distributions of specific lipid and/or protein components, as is the case of domain formation. Vertical asymmetry refers to the difference in molecular composition between the two leaflets of a membrane bilayer. It has been a longstanding question to what extent these two types of asymmetries influence one another. For example, when a domain forms on one leaflet, what impact does it have on the physicochemical properties of the corresponding area directly across from it on the opposite leaflet? In other words, when two areas spanning the bilayer leaflets are coupled, how are their respective properties altered as a result? In the context of phosphoinositide signaling pathways, this is a major question because several PIP mediated signaling events have been associated with the formation of liquid-ordered domains (raft domains).[5–14] The notion that phosphoinositides could be enriched in raft domains has been controversial for decades[15,16] because the predominant acyl chain composition of PIPs – stearoyl-arachidonoyl – is considered too disordered for the lipid to accumulate in raft domains. In an elegant study, Myeong *et al.*[17] recently showed in cells that phosphatidylinositol-4-phosphate (PI(4)P) and -4,5-bisphosphate ($PI(4,5)P_2$) are present in both liquid-ordered (Lo) and liquid-disordered (Ld) phases, with no accumulation preference for either phase. Notably, they also found that $PI(4,5)P_2$ depletion by phospholipase C and the subsequent restoration of $PI(4,5)P_2$ levels was faster in the Lo than in the Ld phase. This finding suggests that the physical state of the phase where a phosphoinositide resides affects the activity of PIP modifying enzymes and potentially other proteins that interact with PIPs. Although the Myeong *et al.* study revealed how cholesterol depletion affects the global distribution of $PI(4,5)P_2$, several unresolved issues regarding the physicochemical mechanisms of raft-associated, PIP-mediated signaling events remain.

While the lipid composition of rafts in the outer leaflet of the plasma membrane has been thoroughly investigated,[18,19] we lack knowledge about inner leaflet raft lipid composition. Consequently, we have virtually no knowledge about the factors that affect PIP distribution between non-raft (Ld) and raft (Lo) regions. The physical properties of an inner leaflet raft domain containing PIPs have not been detailed and it is unclear to what extent PIP interaction with proteins is modulated by a raft *vs.* non-raft residency. While it has been shown for Langmuir films[20] and symmetric lipid vesicles[21–23] that calcium ions and/or cholesterol promote the formation of PIP enriched domains, it is currently unknown how this plays out in an asymmetric lipid bilayer environment exhibiting a lipid raft composition in one of the two leaflets.

To refine our understanding of interleaflet coupling, simplified model systems must be developed that exhibit vertical lipid asymmetry. One common method used to fabricate asymmetric small, large, and giant unilamellar vesicles is the cyclodextrin-catalyzed lipid exchange method.[24–27] However, it is important to

note that the extension of this method to phosphoinositide-containing asymmetric lipid bilayer systems, while probably feasible, has limitations regarding the lipid composition of the inner and outer leaflets of the formed vesicle. More specifically, the extent of asymmetry in the formed vesicles is dependent on the level of favorability between the cyclodextrin pore and the lipid headgroups present.[28] Recently, Enoki and Feigenson introduced a hemifusion-based method to fabricate asymmetric giant unilamellar vesicles (aGUVs) and demonstrated its utility for studying raft phenomena.[29,30] This method involves the Ca^{2+} mediated fusion of a symmetric giant unilamellar vesicle (sGUV) with a solid-supported lipid bilayer (SLB) to obtain an aGUV. The addition of EDTA terminates the hemifusion process and leads to the fission of the aGUVs from the SLB. The inner leaflet of the aGUV has the lipid composition of the sGUV, while the outer leaflet exhibits the SLB lipid composition. One advantage of this method is that it does not rely on the selectivity of cyclodextrins thus generally expanding the breadth of lipid compositions that can be used to create asymmetric giant unilamellar vesicles. Our group recently broadened the scope of the hemifusion method to incorporate anionic lipids, enabling the creation of asymmetric giant unilamellar vesicles that contain phosphatidylserine and we did so using buffers of physiological ionic strength.[31]

The hemifusion process as described by Enoki and Feigenson[29] requires the addition of Ca^{2+} to initiate the SLB/sGUV hemifusion. For anionic lipid-containing SLBs, as in this study, the addition of Ca^{2+} may lead to lipid clustering and potentially macroscopic domain formation. It has been suggested that micron-sized phase separation in the SLB might impact the outer leaflet composition of the formed aGUVs.[30,31] This is because some sGUVs will settle during the hemifusion process on regions (domains) exhibiting one lipid composition, while other sGUVs will interact with areas of the SLB that have a different lipid makeup. Thus, selecting a system where the lipids in the SLB do not phase separate under the hemifusion conditions is desirable to obtain less compositional variation in the outer leaflet of the formed aGUVs. Previously, Ca^{2+} had been the reagent of choice in hemifusion experiments with charge-neutral lipids using low ionic strength buffers.[29,30,32,33] In our recent study where we incorporated phosphatidylserine (PS) into the outer leaflets of aGUVs,[31] we found that the addition of Ca^{2+} ions caused PS to form large, micron-sized clusters in the SLB over the course of a few hours in a physiological ionic strength buffer. Since the timescale of the hemifusion event is <25 minutes, we expected that this macroscopic domain formation would have no impact on the compositional quality of the aGUVs because the hemifusion process is completed before the macroscopic domains form. However, it is still possible that nanoscopic domain formation, which probably precedes macroscopic domain formation, impacts the compositional quality of the aGUVs. To test this and to evaluate whether there are alternative bivalent cations that can be used to initiate the hemifusion process, we investigated whether Mg^{2+} can be used instead of Ca^{2+} to obtain aGUVs. The rationale for this approach is that Mg^{2+} does not induce macroscopic PS clustering. We found that Mg^{2+} can indeed replace Ca^{2+} as the hemifusion initiator. In addition, we observed virtually no differences between the compositional quality of the aGUVs obtained *via* Ca^{2+} or Mg^{2+} initiated SLB/sGUV hemifusion, *i.e.*, even if PS/Ca^{2+} nanodomains exist within the hemifusion time window, they did not affect the compositional quality of the aGUVs.

The optimal system for studying phosphoinositide behavior in asymmetric lipid bilayers should provide for the following experimental freedoms. First, it should offer the opportunity to utilize a diverse range of lipid compositions for the PIP-containing leaflet. Second, the experimental approach should be able to accommodate lipid systems with phosphatidylinositol (PI) or any of the seven PIP species. Lastly, the system places PIP lipids in the outer leaflet of the vesicle to make studies aimed at investigating PIP interactions with cations and proteins possible. The hemifusion method is principally suitable for the fabrication of such systems. However, since the interaction of bivalent cations with a particular anionic lipid will depend on the chemical structure of the lipid's headgroup, it is possible that the optimal hemifusion conditions will deviate for particular anionic lipids from those identified for PS. PI(4,5)P_2 has an approximately −4 charge at physiological pH[34] and has been shown to react strongly with Ca^{2+} ions to form macroscopic domains.[20,35] These domains show remarkable thermal stability, persisting at temperatures as high as 80 °C.[23] On the other hand, Mg^{2+} does not induce micron-sized PI(4,5)P_2 domain formation (although it might form nano-sized domains). Also, the interaction between the PI(4,5)P_2 headgroup and Mg^{2+} is significantly weaker at physiological ionic strength than what is observed for buffer conditions with lower ion concentrations.[23,36,37]

In this paper, we present data from applying the hemifusion method, using our adapted approach for buffers with physiological ionic strength,[31] to a system containing phosphatidylinositol-4,5-bisphosphate (PI(4,5)P_2), a lipid with very complex physicochemistry[38–40] and of crucial biological importance.[41,42] For Ca^{2+} mediated hemifusion, we observed a broad compositional distribution in the formed aGUVs. This is attributed to Ca^{2+} induced clustering of PI(4,5)P_2, leading to macroscopic domain formation. Hemifusion of sGUVs with a laterally heterogeneous SLB results in some sGUVs interacting with PI(4,5)P_2 enriched regions (domains), while others settle on regions devoid of PI(4,5)P_2. Consequently, some of the formed aGUVs contain large quantities of PI(4,5)P_2, whereas others will exhibit only small amounts. To address this issue, we explored the possibility of using Mg^{2+} as the hemifusion initiator, as it is known to cluster PI(4,5)P_2_ to a much lesser extent.[22] We find that the replacement of Ca^{2+} with Mg^{2+} as the hemifusion initiator leads indeed to a significantly improved compositional homogeneity throughout asymmetric bilayer leaflets.

2 Materials & methods

2.1. Materials

Porcine brain L-α-phosphatidylinositol-4,5-bisphosphate (brain-PI(4,5)P_2) ammonium salt, 1,2-dioleoyl-*sn*-glycero-3-phosphocholine (DOPC), and 1-oleoyl-2-[6-(4-(dipyrromethene borondifluoride)butanoyl)amino]hexanoyl-*sn*-glycero-3-phosphoinositol-4,5-bisphosphate (TF-PI(4,5)P_2) ammonium salt were obtained as powders from Avanti Polar Lipids (Alabaster, Alabama) and used as received. 1,1′-Dioctadecyl-3,3,3′,3′-tetramethylindodicarbocyanine (DiD′) 4-chlorobenzene-sulfonate salt was obtained as a powder from Invitrogen™ (Waltham, MA). Nunc Lab-Tech II 8-well chambered coverglasses were purchased from Thermo Fisher (Waltham, MA, USA). Wide-orifice pipette tips were created by cutting the ends off standard plastic pipette tips. Bachmore© 50g artist-grade tracing paper was purchased from Amazon (Seattle, WA, USA). Liquinox was

obtained from Alconox (White Plains, NY, USA). Sodium chloride, potassium chloride, calcium chloride, magnesium chloride, disodium ethylenediamine tetraacetic acid (Na_2EDTA), 4-(2-hydroxyethyl)-1-piperazineethanesulfonic acid (HEPES), sucrose, and glucose were obtained in high purity grades either through Fisher Scientific (Fairlawn, NJ, USA) or Sigma Aldrich (St. Louis, MO, USA). HPLC grade chloroform, ethanol, isopropanol, and methanol were also obtained through Fisher Scientific (Fairlawn, NJ, USA). Deionized water (18.2 MΩ cm^{-1}) was obtained using a RODI (Aztec, NM, USA) high-purity water system.

Phosphoinositide stock solutions were prepared by dissolving the lipid powder in a mixture of chloroform, methanol, and water in a ratio of 20 : 9 : 1 by volume. DOPC stocks were dissolved in a 2 : 1 mixture of chloroform and methanol by volume. The purity of lipid stock solutions was monitored continually by thin-layer chromatography. Concentrations of the phospholipid stock solutions were determined using an inorganic phosphate assay.[43] The DiD′ stock solution was prepared in HPLC grade ethanol. The fluorophore (DiD′ and TF-PI(4,5)P_2) stock solution concentrations were approximated using the Beer–Lambert relationship by taking absorbance measurements in methanol at 646 nm and 496 nm, respectively, and using the corresponding extinction coefficients (ε). The ε of DiD′ was obtained from the reagent lot's certificate of analysis ($\varepsilon = 250\,000$ $M^{-1}cm^{-1}$), while the ε of TF-PI(4,5)P_2 was obtained from Avanti Polar Lipids ($\varepsilon = 97\,000$ $M^{-1}cm^{-1}$). All lipid stock solutions and dyes were stored at −20 °C away from light.

2.2 Fabrication of asymmetric giant unilammellar vesicles

The procedure to fabricate asymmetric Giant Unilamellar Vesicles (aGUVs) using the hemifusion method requires three principal steps: Generation of symmetric Giant Unilamellar Vesicles (sGUVs), fabrication of solid supported lipid bilayers (SLB) from small unilamellar vesicles, and the hemifusion of the sGUVs with the SLB.

2.2.1 Generating symmetric giant unilamellar vesicles. Methods for obtaining a high yield of sGUVs will differ based on the desired lipid components. For the sGUVs representing the inner leaflet composition of the studied aGUVs, we used a molar composition of DOPC/DiD′ (99.02/0.08 mol%). For sGUVs representing the outer leaflet, we used a molar composition of DOPC/brain-PI(4,5)P_2/TF-PI(4,5)P_2 (95/4.94/0.06 mol%). A 0.5 mM total lipid stock solution of the desired inner leaflet composition was created. Separately, a 1 mM total lipid stock solution of the desired outer leaflet composition was prepared to a final volume of 600 μL prior to making the inner leaflet control sGUVs and the small unilamellar vesicles (SUVs) required to prepare the SLB. sGUVs were prepared using the PAPYRUS method with tracing paper as described by the Subramaniam group, modified for our purposes to exclude PEG lipids, incorporate a physiological concentration of salt, and include PI(4,5)P_2.[44,45]

In brief, a piece of tracing paper was first cleaned by submerging it in chloroform for 30 min and gently stirring every 10 min. This was then repeated with a fresh volume of chloroform. Afterwards, the chloroform was replaced with DI water and the previous process was repeated for another 30 min. Next, the paper was dried in a vacuum oven around 60 °C at 15 mmHg until dry. Once dry, two 6.35 mm diameter circular cutouts were removed from the paper using a single

hole hole-puncher and coated with a 10 μL solution of either the outer leaflet lipid stock solution or the inner leaflet lipid stock solution. After applying this mixture, the paper cutout was placed back into the vacuum oven for 30 min. After drying, the cutout with the DOPC/DiD′ lipid mixture was placed in the bottom of a microwell plate at room temperature. The cutout with the DOPC/PI(4,5)P_2/TF-PI(4,5)P_2 mixture was placed in a 2 mL Eppendorf vial warmed to 49 °C. The following steps were taken to prepare both the inner and outer leaflet sGUVs, except all buffers used to make the PI(4,5)P_2 sGUVs were first warmed to 49 °C. 142.5 μL of 105 mM sucrose was added to the well containing the paper cutout, followed by 7.5 μL of a concentrated buffer solution containing 2.0 M NaCl, 1.0 M KCl, 0.020 M Na_2EDTA, 0.50 M HEPES pH = 7.4 10 min later to obtain an approximately 100 mM sucrose, 97 mM NaCl, 50 mM KCl, 1.0 mM Na_2EDTA, 25 mM HEPES, pH 7.4 buffer inside and outside of the formed sGUVs. The sGUVs were then collected after 110 min. To collect sGUVs after their formation, a pipette with a wide orifice tip was used to aspirate and dispense 150 μL of the solution 6 times before removing the entire solution. The osmolality of the sucrose + concentrated buffer solution was measured with an Advanced Instruments model 3300 Micro Osmometer (Norwood, MA, USA). All other buffers used in this study were adjusted to within ±2 mOsm kg^{-1} of this reading using either a 2 M NaCl solution (to adjust up) or DI water (to adjust down).

2.2.2 Preparing BSA-coated cover glasses. sGUV controls were imaged in chambered coverglasses coated with bovine serum albumin (BSA) to prevent the GUVs from rupturing upon contact with the glass. The coating procedure began with a thorough cleaning of the coverglass. The chambers were first rinsed three times in the following order: DI water, ethanol, isopropanol, ethanol, DI water. Next, the coverglass was sonicated for 15 min in dilute Liquinox detergent (around 2% (w/v) in DI water) at 69 °C in a Branson 1510 water bath sonicator (Brookfield, CT). Once done, the coverglass was rinsed again in the same order as before but finished with copious amounts of DI water. The coverglass was then dried under nitrogen gas and primed for BSA coating by filling each chamber with 0.01 M NaCl. After 40 min, 0.01 M NaCl was replaced with 1 mg per mL BSA in 0.01 M NaCl at pH = 5.0 to apply the BSA coating. After a minimum 3 h period, the coverglass was rinsed with copious DI water to remove excess BSA unbound from the glass surface. The DI water present in the BSA coated chambers was completely removed before the addition of sGUVs.

2.2.3 Fabrication of solid supported lipid bilayers. The solid-supported lipid bilayer composition is representative of the outer leaflet composition of the aGUVs formed using the hemifusion method. We used the same lipid stock solution to prepare both the outer leaflet sGUV controls and the small unilamellar vesicles (SUVs) used to create the SLB. The remaining 590 μL of the 1 mM total lipid stock solution containing PI(4,5)P_2 was dried under a steady stream of nitrogen gas at an elevated temperature. Following this, the vial containing the dried mixture is placed in a vacuum oven for 30 min to remove any residual solvent trapped between the layers of dried lipid. Once dry, the lipids are resuspended in a 97 mM NaCl, 100 mM KCl, 1 mM Na_2EDTA 25 mM HEPES, pH 7.4 buffer warmed to 49 °C and vortexed to create an opaque suspension of multilamellar vesicles (MLVs). The MLVs were then transferred from the vial into an Eppendorf tube and sonicated using a Sonics Vibra-Cell VCX130 Ultrasonic Processor tip sonicator (Newton, CT, USA), where an amplitude of 50% was applied to the vesicles in 15 s pulses (15 s on,

15 s off) for 30 min. After 30 min, a clear suspension of small unilamellar vesicles (SUVs) with an average diameter centered around 50–60 nm was retrieved. SUV diameters were confirmed using the dynamic light scattering function of a Malvern Zetasizer instrument (Malvern, Worcestershire, UK). These vesicles were then diluted fivefold using the resuspension buffer before use.

Before using the SUVs to form the SLBs, another chambered coverglass was first cleaned using the same method as described for the BSA-coated coverglass, but in this case, after drying the cleaned coverglass with nitrogen gas, it was plasma-cleaned under oxygen for 1.5 min using an LF-5 Plasma System (Mercator Control Systems, PVA TePla AG, Wettenberg, Germany). Immediately after plasma cleaning, a 0.5 mL aliquot of the diluted SUVs was added to two or three of the 8 chambers to begin SLB formation. In this process, the SUVs in each chamber settle to the bottom and fuse to form a planar bilayer. The SLBs were left to form, protected from light, for 20 min at room temperature. To remove residual unruptured vesicles and debris from the solid-supported lipid bilayer surface, 500 μL of resuspension buffer was added to the chamber and gently aspirated three times, discarding the buffer afterward. This process was repeated with fresh buffer two additional times, resulting in a total of nine aspirations. At the end, approximately 500 μL of buffer remained in the chamber. The quality (completeness) of the SLB was checked using fluorescence microscopy.

2.2.4. Hemifusion of symmetric giant unilamellar vesicles with supported lipid bilayers. Asymmetric GUVs were prepared using the hemifusion method we adapted in a recent paper for high salt concentrations.[31] In this procedure, 5 × 5 μL DOPC/DiD′ (99.9/0.1 mol%) sGUVs aliquots were added using a wide orifice pipette tip to a chamber containing a DOPC/PI(4,5)P_2/TF-PI(4,5)P_2 (95/5/0.06 mol %) SLB in 97 mM NaCl, 100 mM KCl, 1 mM Na_2EDTA, 25 mM HEPES, pH 7.4 (resuspension buffer). After waiting 10 min for the sGUVs to settle to the bottom of the chamber, hemifusion between the sGUVs and SLB was induced by adding 120 μL of 20 mM MCl_2 (M = Ca^{2+} or Mg^{2+}), 100 mM NaCl, 70 mM KCl, 25 mM HEPES, pH = 7.4 buffer. After waiting ~23 min for hemifusion to progress, 250 μL of a 20 mM Na_2EDTA, 100 mM NaCl, 76 mM KCl, 25 mM HEPES, pH 7.4 buffer was added to chelate all of the bivalent cations and end the hemifusion process. A final 10 min period transpired before imaging to allow the system to equilibrate. Fresh sGUV controls were prepared and used on the same day as the hemifusion experiment. To ensure that any variations in results were directly attributable to the identity and concentration of the bivalent cations used to induce hemifusion, multiple experimental conditions were tested across different SLBs using the same control sGUV populations.

2.3 Fluorescence imaging

GUVs and SLBs images were captured on a Zeiss LSM510 confocal microscope (Oberkochen, Germany). SLBs and aGUVs were imaged in the chambers they were prepared in. sGUVs were imaged on BSA-coated coverglass by adding 20–30 μL of the sGUVs to the chamber, followed by 250 μL of a 100 mM glucose, 97 mM NaCl, 50 mM KCl, 1 mM Na_2EDTA, 25 mM HEPES, pH 7.4 buffer. Adding the glucose buffer after adding the GUVs helps the vesicles settle on the bottom and provides a better imaging contrast. All GUV images were obtained with plan-apochromat 63× magnification oil immersion objective. For the TF-channel, a 488 nm Ar

laser with 505 nm long pass filter was used. For the DiD′ channel, a 633 nm HeNe laser with a 650 nm long pass filter was utilized. Unless otherwise specified, all GUV images were taken by capturing a single frame at the equator of the vesicle. Collected images were later processed in ImageJ by first applying the Gaussian blur filter with a radius of 1 μm, followed by an ImageJ code created by Dr Thais Enoki.[29] Fluorescence intensity data for each individual sGUV and aGUV were obtained by averaging the peak intensity profiles of 360 line scans in ImageJ and then plotted in Wolfram Mathematica©. Additional data plotting and statistics were performed in Excel and Origin Lab® 64 bit.

2.4 Analyzing asymmetric giant unilamellar vesicles

To determine the average fluorescence intensity of a vesicle, the ImageJ code generates 360 rays that radiate from the center of the vesicle image. These rays trace the perimeter of the vesicle, capturing the peak fluorescence intensity at 360 points along the edge. These peak intensities are then averaged together to give an average fluorescence intensity of a given vesicle. The average of all fluorescence intensities for each control population (TF-PI(4,5)P_2 controls and DiD′ controls) and aGUV population were taken. Any vesicles that fell outside two times the standard deviation of the channel average were discarded as outliers. A vesicle's DiD′ or TF-PI(4,5)P_2 intensity is chiefly dependent on the fraction of DiD′ or TF-PI(4,5)P_2 present in it. Theoretically, aGUVs that experienced complete outer leaflet exchange with the SLB should have half the fraction of DiD′ and TF-PI(4,5)P_2 as their sGUV counterparts, meaning their DiD′ and TF-PI(4,5)P_2 intensities should be half that of the sGUVs and with half the distribution width of the sGUVs. We term this region the 'passing range'.

We also used two other parameters to assess the quality of the formed aGUVs: leaflet exchange (P^{ex}) and percentage agreement ($P^{a\%}$). P^{ex} is defined as how much DiD′ diffused out of or TF-PI(4,5)P_2 incorporated into the aGUV relative to the control GUVs and can be calculated as follows:

$$\text{Exchange (TF-PI}(4,5)\text{P}_2) = P^{ex}_{TF} = \frac{I_a}{I_c/2} \quad (1)$$

$$\text{Exchange (DID)} = P^{ex}_{DID} = 2\left(1 - \frac{I_a}{I_c}\right) \quad (2)$$

where I_a represents the average intensity of an aGUV channel and I_c represents the average intensity of all the symmetric control GUVs in the corresponding channel. $P^{a\%}$ is a simple parameter used to estimate how well the exchange percent values for each channel are aligned. $P^{a\%}$ can be calculated as shown below:

$$\text{Percentage agreement} = P^{a\%} = 100\% - [|P^{ex}_{TF} - P^{ex}_{DiD'}| \times 100].$$

A $P^{a\%}$ value of 100% for a given aGUV would mean that the amount of DiD′ exchanged with TF-PI(4,5)P_2 is equal, while a value below 100% indicates incomplete exchanges for one or both leaflets.

To summarize, an aGUV was considered to have undergone complete exchange with the proximal SLB leaflet only if the following conditions were met:

(1) Both the green (TF) and the red (DiD′) channel average fluorescence intensity values of the aGUV fell within the passing range.

(2) The leaflet exchange ratio for each channel of an aGUV fell within ±0.30 of complete outer exchange.

(3) The percentage agreement between the red and green channels in the aGUV fell within ±30%.

3 Results and discussion

3.1 Evaluation of the quality of solid supported PI(4,5)P_2/PC bilayers upon addition of Ca^{2+} or Mg^{2+}

The morphology and integrity of the solid-supported lipid bilayer used for the hemifusion and the time course of domain development, if it occurs, upon the addition of bivalent cations is an important factor for the quality of the aGUVs. Fig. 1 displays images of PI(4,5)P_2/PC supported lipid bilayers before and after either Ca^{2+} or Mg^{2+} was added. The images were taken less than five minutes after adjusting the bivalent cation concentration to the indicated amount. As seen in Fig. 1b, within moments, Ca^{2+} causes PI(4,5)P_2 to form long "finger-like" domains consisting of what appears to be multiple smaller, circular areas. Meanwhile, no domains appear to form in the SLB containing Mg^{2+}. Longer time scales result in the domains becoming larger and more circular.

3.2 Comparison of aGUVs obtained through hemifusion initiated with either 6 mM Ca^{2+} or Mg^{2+}

Fig. 2 shows DOPC and DOPC/brain PI(4,5)P_2 sGUVs in the left column, while the right hand columns display aGUVs that contain PI(4,5)P_2 on the outer leaflet and PC on the inner leaflet using either 6 mM Ca^{2+} or 6 mM Mg^{2+} as the initiator for hemifusion. We selected these concentrations to serve as a baseline of comparison to the method we developed for PS/PC aGUVs at physiological salt concentrations.[31] While these bivalent cation concentrations significantly exceed their physiological levels in cells, the addition of EDTA (hemifusion termination step) effectively masks these cations after the hemifusion is completed.

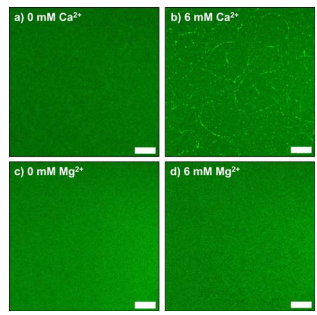

Fig. 1 Images of 95/4.94/0.06 mol% DOPC/brain-PI(4,5)P_2/TF-PI(4,5)P_2 solid-supported lipid bilayers. The left column displays SLBs with a buffer composition of 97 mM NaCl, 100 mM KCl, 1 mM Na_2EDTA 25 mM HEPES, pH 7.4 (resuspension buffer) prior to adding bivalent cations. The right column displays the same area of the SLB from the left column with either 6 mM Ca^{2+} or 6 mM Mg^{2+} present. (a) 0 mM Ca^{2+} (b) 6 mM Ca^{2+} (c) 0 mM Mg^{2+} (d) 6 mM Mg^{2+}. We accounted for the presence of EDTA by assuming 1 : 1 stoichiometry between the bivalent cation and EDTA. Scale bar = 20 μm.

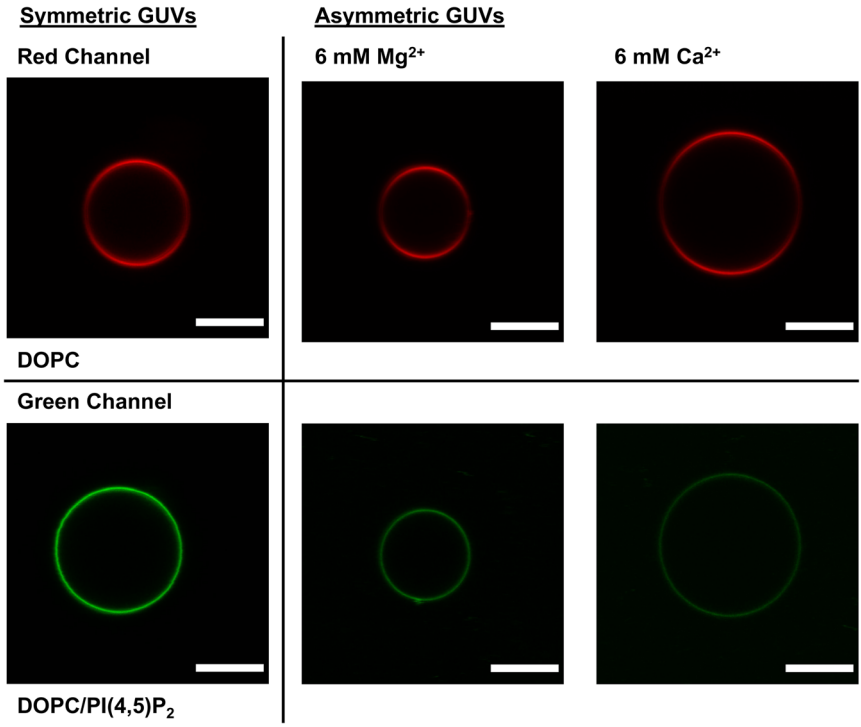

Fig. 2 Images of symmetric control GUVs (left column) and asymmetric GUVs (right column) prepared with either 6 mM Mg^{2+} or 6 mM Ca^{2+} as indicated. Scale bar = 10 μm. sGUV controls were prepared in 100 mM sucrose but were imaged in 100 mM glucose for a total buffer composition of 100 mM saccharide, 97 mM NaCl, 50 mM KCl, 1 mM Na_2-EDTA, 20 mM HEPES, pH = 7.4 on either side of the vesicle bilayer. aGUVs were imaged above the SLB after hemifusion in the resuspension buffer plus the indicated amount of bivalent cation and ~7 mM Na_2EDTA. Vesicles prepared with DiD′ appear dimmer at the equator due to a well-known polarization artifact arising from the properties of the fluorophore and are not due to phase separation in a pure DOPC bilayer.

Fig. 3 shows the processed intensity data (see methods section for details) for the sGUV controls and the aGUVs obtained through Ca^{2+} initiated hemifusion. Even after removing outliers, we found that the sGUV controls (Fig. 3a, left) containing PI(4,5)P_2 (green controls) have a wider distribution in fluorescence intensities compared to the pure DOPC sGUVs (red control). While the general fragility of GUVs with high (>5 mol%) levels of PI(4,5)P_2 (ref. 46) might be one of the reasons for the broader intensity distribution, it cannot be ruled out that interactions between PI(4,5)P_2 and the cellulose of the PAPYRUS during the swelling process may also be a contributing factor for the varying levels of PI(4,5)P_2 in the sGUVs. It is important to note that the PI(4,5)P_2/PC sGUVs are solely used to obtain fluorescence intensity values for a lipid bilayer so that the degree of exchange for the aGUVs can be evaluated.

The right side of Fig. 3a shows the normalized intensity distribution for DOPC/PI(4,5)P_2/TF-PI(4,5)P_2 (outer leaflet/green channel) and DOPC/DiD′ (inner leaflet/red channel) aGUVs. Since the aGUVs contain each lipid mixture only in one

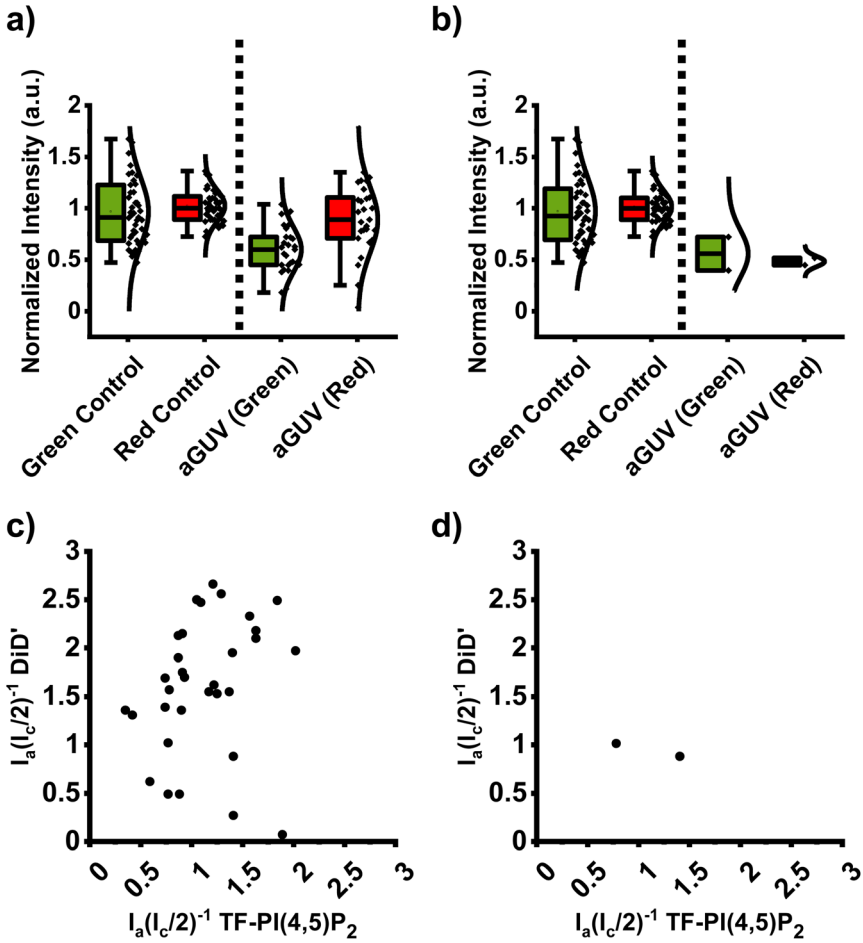

Fig. 3 DOPC/DiD (inner leaflet, red channel): DOPC/PI(4,5)P_2/TF-PI(4,5)P_2 (outer leaflet, green channel) asymmetric giant unilamellar vesicles prepared using 6 mM Ca^{2+} as the hemifusion initiator. (a) Comparison of sGUV controls for the green (DOPC/PI(4,5)P_2/TF-PI(4,5)P_2; $N = 51$) and red (DOPC/DiD′; $N = 47$) channels to the corresponding fluorescence channels of imaged aGUVs ($N = 32$) across 6 separate experiments. (b) The range-passing aGUVs (see text) from the samples presented in panel A. (c) Cross-correlation of the two channels for individual aGUVs. A "perfect" aGUV would be found at the data point (1,1) which corresponds to a completely exchanged outer leaflet and no artifacts like multi-lamellarity. (d) Cross-correlation of the two channels for the range-passing aGUVs. sGUV buffer: 97 mM NaCl, 100 mM KCl, 1 mM Na_2EDTA, 25 mM HEPES pH = 7.4 buffer. aGUV buffer after hemifusion: 97 mM NaCl, 100 mM KCl, 7 mM Na_2EDTA, 25 mM HEPES pH = 7.4 buffer. The controls displayed in (a) and (b) are the same experiments and are reproduced for comparison.

leaflet (as opposed to both leaflets in sGUVs), the intensities for the aGUVs are expected to be half of the intensity values for the corresponding sGUVs. While the median for the aGUV TF-PI(4,5)P_2 (outer leaflet) intensities is near the expected 0.5 intensity value, the DiD′ median intensity is slightly above 0.5 of the corresponding sGUV intensity and the distribution is broader than that observed for the TF-PI(4,5)P_2 (green) channel.

To identify those aGUVs that are artifact-free and exhibit a near complete DOPC/DiD′ inner leaflet, we analyzed the scatter plot in Fig. 3c, which correlates the fluorescence intensities of DiD′ and TF-PI(4,5)P_2 in aGUVs. Please note that the *x*-axis in Fig. 3c and d represents the fraction of the sGUV leaflet exchanged for the TF-PI(4,5)P_2 containing lipid mixture, while the *y*-axis represents the fraction of DiD′ leaflet remaining in the formed aGUV (the same applies to Fig. 4, 5c and d). By dividing the aGUV fluorescence intensities (I_a) for each channel by half of the corresponding sGUV intensities ($0.5I_c$), we obtain a value of "1" for a complete leaflet. This normalization places the "near perfect" aGUVs (outer sGUV leaflet completely hemifusion exchanged) around the (1,1) data mark on the scatter plot. It is clear from the scatter plot that many of the aGUVs don't fulfill the requirement of being close to the (1,1) mark. Furthermore, even for an incomplete exchange of the outer leaflet, the sum of the TF-PI(4,5)P_2 and DiD′ values should yield "2" since this corresponds to a unilamellar vesicle (single lipid bilayer). However, for several aGUVs the sum of the two values is significantly above "2", suggesting that the quality of these aGUVs has been compromised.

Vesicles can deviate from expected hemifusion values for multiple reasons. The most obvious reason is multi-lamellarity. Multilamellar vesicles present in the aGUV population can distort the observed distribution of fluorescence intensities since the presence of multiple bilayers intrinsically results in unpredictable fusion properties. While the algorithm used to determine the GUV fluorescence intensity values filters multilamellar symmetric giant vesicles out, it may fail to identify asymmetric giant vesicles that have partially exchanged their outermost leaflet. Another important aspect to consider is that in particular, TF-PI(4,5)P_2 is subject to quenching when the (local) fluorophore density changes, *e.g.*, due to the formation of domains (even though macroscopic domains are not discernible, nanoscopic domains might exist). This will obscure any quantitative analysis that is based on fluorescence intensities. Another reason is the presence of domains in the solid-supported lipid bilayer as can be seen in Fig. 1 for the Ca^{2+} initiated hemifusion. As the added symmetric GUVs make contact with the SLB, some vesicles will settle on regions enriched in PI(4,5)P_2, while others will interact with regions deficient in PI(4,5)P_2. Since the fluorescent probe used to monitor the extent of exchange for the SLB was a chain-labeled PI(4,5)P_2 molecule, this will lead to aGUVs that are either enriched or depleted in TF-PI(4,5)P_2, depending on whether the sGUV interacted with a domain or not.

To filter for the aGUVs that show fluorescence intensities for both channels within an acceptable range around half the corresponding intensity of the sGUVs, we utilized a data analysis method introduced in our recent paper on PS containing aGUVs.[31] Asymmetric GUVs with a fluorescence intensity in each channel that fall within one-half the average and standard deviation of their corresponding controls are considered 'range-passing', *i.e.*, in both channels, the acceptable intensity spread is one-half the intensity spread observed for the corresponding sGUV. Out of 32 imaged aGUVs across 6 repeat experiments, only two aGUVs prepared with 6 mM Ca^{2+} as the hemifusion initiator were range-passing (Fig. 3b). Consequently, those two aGUVs exhibit data points in the scatter plot near the (1,1) mark, however, overall, the yield of high quality aGUVs when Ca^{2+} is used as the hemifusion initiator, is unsatisfactory.

To test whether other bivalent cations yield better hemifusion results when PI(4,5)P_2 is present in the SLB, we expanded our study to Mg^{2+}. Fig. 4 shows the

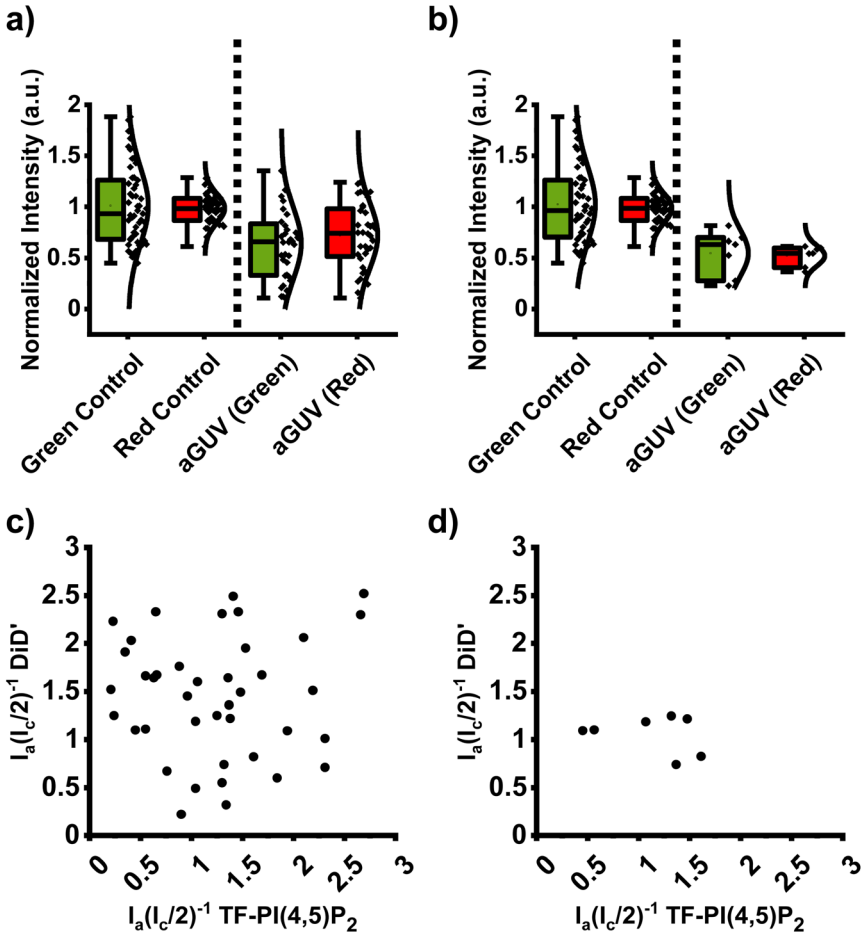

Fig. 4 DOPC/DiD (inner leaflet, red channel):DOPC/PI(4,5)P_2/TF-PI(4,5)P_2 (outer leaflet, green channel) asymmetric giant unilamellar vesicles prepared using 6 mM Mg^{2+} as the hemifusion initiator. (a) Comparison of sGUV controls for the green (TF-PI(4,5)P_2; $N = 49$) and red (DiD′; $N = 46$) channels to the corresponding fluorescence channels of imaged aGUVs ($N = 40$) across 5 separate experiments. (b) the range-passing aGUVs from the samples presented in (a). (c) Cross-correlation of the two channels for individual aGUVs. A "perfect" aGUV would be found at the data point (1,1) which corresponds to a completely exchanged outer leaflet and no artifacts like multi-lamellarity. (d) Cross-correlation of the two channels for the range-passing aGUVs. sGUV buffer: 97 mM NaCl, 100 mM KCl, 1 mM Na_2EDTA, 25 mM HEPES pH = 7.4 buffer. aGUV buffer after hemifusion: 97 mM NaCl, 100 mM KCl, 7 mM Na_2EDTA, 25 mM HEPES pH = 7.4 buffer. The controls displayed in (a) and (b) are the same experiments and are reproduced for comparison.

results for hemifusion initiated with 6 mM Mg^{2+}. Fig. 4a displays the fluorescence intensities for both channels, while Fig. 4c displays the corresponding scatter plot. Also in this case, many aGUVs are distant from the high-quality (1,1) exchange value. Fig. 4b and d show the data after the range-passing algorithm (described above) was applied. The number of vesicles that were range-passing was 7 out of 40 imaged vesicles giving a yield of approximately 18%. For the TF-PI(4,5)P_2 channel, some of the data points that are range passing are distant

from the (1,1) data point. Since the distribution of the $PI(4,5)P_2$ containing sGUVs is quite broad, more aGUVs become range-passing even though only 50% of the outer leaflet has been exchanged. Overall, the quality of the aGUVs when using 6 mM Mg^{2+} instead of Ca^{2+} is improved, however, a greater yield is still desirable.

We were interested to see whether a lower concentration of Mg^{2+} would be sufficient to induce hemifusion in a system that contains $PI(4,5)P_2$ and whether this would result in a higher yield of high-quality aGUVs. There are two reasons

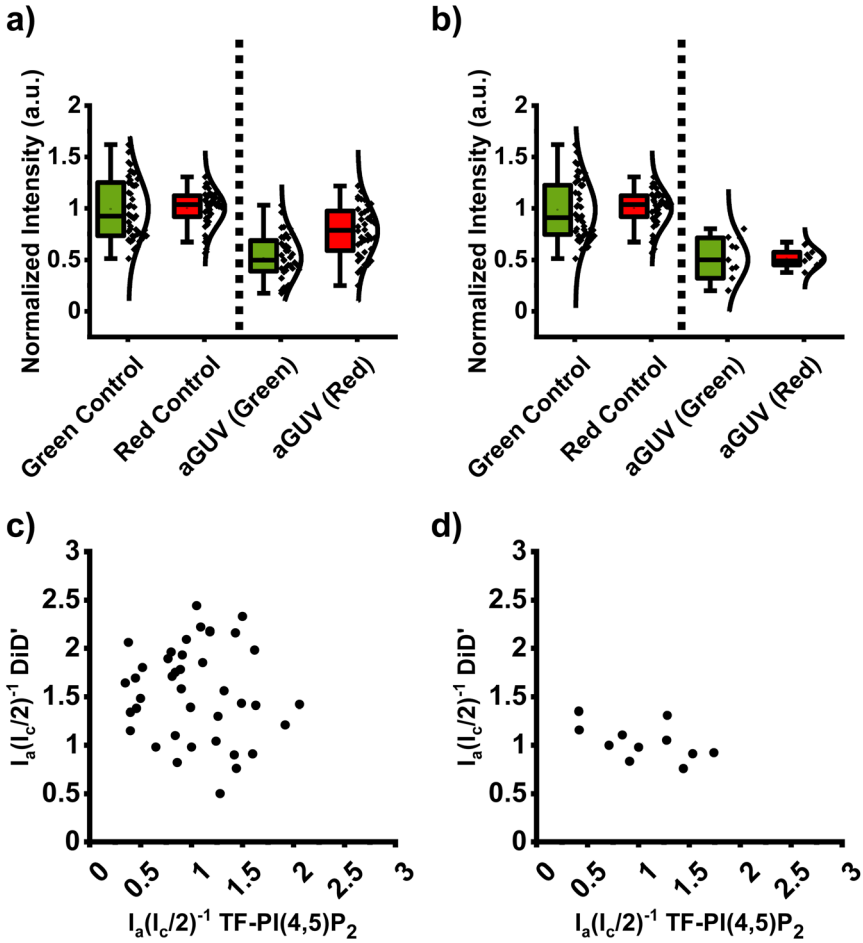

Fig. 5 DOPC/DiD (inner leaflet, red channel): DOPC/$PI(4,5)P_2$/TF-$PI(4,5)P_2$ (outer leaflet, green channel) asymmetric giant unilamellar vesicles prepared using 1 mM Mg^{2+} as hemifusion initiator. (a) Comparison of sGUV controls for the green (TF-PI(4,5)P2; $N = 47$) and red (DiD′; $N = 47$) channels to the corresponding fluorescence channels of imaged aGUVs ($N = 40$) across 5 separate experiments. (b) The range-passing aGUVs from the samples presented in (a). (c) Cross-correlation of the two channels for individual aGUVs. A "perfect" aGUV would be found at the data point (1,1) which corresponds to a completely exchanged outer leaflet and no artifacts like multi-lamellarity. (d) Cross-correlation of the two channels for the range-passing aGUVs. sGUV buffer: 97 mM NaCl, 100 mM KCl, 1 mM Na_2EDTA, 25 mM HEPES pH = 7.4 buffer. aGUV buffer after hemifusion: 97 mM NaCl, 100 mM KCl, 7 mM Na_2EDTA, 25 mM HEPES pH = 7.4 buffer. The controls displayed in (a) and (b) are the same experiments and are reproduced for comparison.

for this: First, a lower Mg^{2+} concentration limits the interference from $PI(4,5)P_2$/Mg^{2+} domains that may exist at the nanoscopic level. Second, to anticipate experimental difficulties that will arise when the aGUVs are used in experiments to model bivalent cation-induced domain formation of anionic lipids. To stop hemifusion, EDTA is added to the suspension, which binds the Mg^{2+} and leads to the detachment of the aGUVs from the SLB. For experiments aimed at studying the effect of Ca^{2+} on $PI(4,5)P_2$ domain formation in asymmetric lipid bilayers, the addition of Ca^{2+} will set free the EDTA bound Mg^{2+} since Ca^{2+} binds EDTA more strongly than Mg^{2+}. To use the aGUVs containing $PI(4,5)P_2$ as inner leaflet plasma membrane models, the ideal scenario would be one where the salt concentration more closely resembles that of the cytoplasm post-hemifusion. Therefore, using 1 mM Mg^{2+} instead of 6 mM will yield, after the addition of Ca^{2+} (over titration of EDTA), a Mg^{2+} concentration that more closely resembles cellular concentrations (0.5–1 mM).

Fig. 5 shows the data for aGUVs with an outer leaflet composition of DOPC/brain-$PI(4,5)P_2$/TF-$PI(4,5)P_2$ (95/4.94/0.06 mol%) using 1 mM Mg^{2+} to initiate hemifusion. Fig. 5a and b show that the yield of aGUVs is generally very high. Furthermore, nine aGUVs were considered range-passing out of 40 total for an approximately 23% yield, which is notably higher than in either of the other conditions. The distribution of P^{ex} values of both the green and red channels appear tighter than in either of the 6 mM Ca^{2+} or 6 mM Mg^{2+} conditions, as shown in Fig. 5c. Of the nine aGUVs that are range-passing, six fit our criteria of P^{ex} and $P^{a\%}$ values of less than 30%.

3.3 Evaluating aGUV quality using DiD′/TF-$PI(4,5)P_2$ exchange agreement value

In Fig. 3–5, we we are utilizing the formula $(I_a/(I_c/2)^{-1}$ for both DiD and TF-$PI(4,5)P_2$ to evaluate the quality of the exchange. In the case of the DiD containing leaflet this

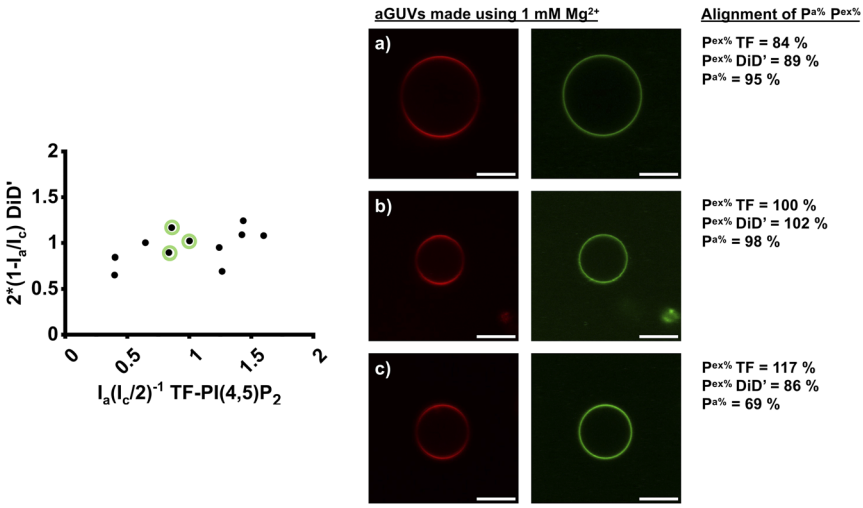

Fig. 6 Identification of the aGUVs with both, DiD′ and TF-$PI(4,5)P_2$, fluorescence intensity exchange P^{ex} are within 30% of each other (green circle identifies the selected aGUVs). Exchange agreement = $P^{a\%} = 100\% - [(P^{ex}(TF) - P^{ex}(DiD')) \times 100\%]$.

calculation determines the fraction of the DiD leaflet remaining rather than the fraction of DiD leaflet exchanged. In Fig. 6 eqn (2) is utilized to calculate exchange DiD. A major strength of using fluorescence microscopy of GUVs is that one can select for further studies the aGUVs that meet certain quality criteria, namely unilamellarity and a near perfect exchange of the outer leaflet. In Fig. 3–5, we based our yield calculation on how well each leaflet matches one-half the average and standard deviation of its corresponding symmetric control population. Doing so identifies a number of aGUVs that fall within a range that matches the theoretical leaflet composition of an ideal aGUV prepared from those symmetric lipid bilayers. In Fig. 6, we reproduce Fig. 5d (please note that the *y*-axis is changed to represent the fraction of exchanged DiD′ leaflet) and highlight those data points that fulfill the requirement that the data for both channels are within ±30% of each other and show the images for three of these aGUVs. The $P^{a\%}$ aGUV quality value shows excellent exchange and bilayer properties. Our desired outer leaflet composition, as determined by the lipid composition of the SLB used, was DOPC/brain-PI(4,5)P_2 (95/4.94/0.06 mol%). Thus, we can be reasonably confident that we obtained four vesicles that approximate the desired inner and outer leaflet asymmetric GUV composition of 100 mol% DOPC and 95/4.95 DOPC/PI(4,5)P_2, respectively. By multiplying the desired leaflet compositions by the P^{ex} values for each channel one can approximate the asymmetric vesicle composition, however, this assumes that the TF-PI(4,5)P_2 amount accurately reflects the overall PI(4,5)P_2 concentration. For the aGUVs prepared in 1 mM Mg^{2+}, the variation in PI(4,5)P_2 spans from ~3 mol% to ~5 mol% for the leaflet. This 2 mol% difference is equal to the range of PI(4,5)P_2 concentrations believed to exist on the plasma membrane (1–2 mol% across the plasma membrane bilayer). We chose a higher concentration of PI(4,5)P_2 to avoid potential quenching artifacts from TF-PI(4,5)P_2 which occur as a result of interactions with bivalent cations at plasma membrane concentrations of PI(4,5)P_2.[22,23]

4 Conclusions

We investigated the suitability of Ca^{2+} or Mg^{2+} initiated hemifusion of a PC sGUV with a mixed PC/PI(4,5)P_2 SLB to obtain aGUVs with the phosphoinositide species in the outer leaflet. We found that using 6 mM Ca^{2+} to initiate hemifusion in a system where PI(4,5)P_2 was present in the supported lipid bilayer resulted in the formation of micron-sized domains which affected the quality of aGUVs produced by creating many aGUVs that were either enriched or lacking in TF-PI(4,5)P_2 content. By relying on a known tendency of Mg^{2+} to cluster PI(4,5)P_2 to a much lesser extent than Ca^{2+}, we were able to slightly improve our yield of usable aGUVs using 6 mM Mg^{2+} as the initiator. However, when applying the most stringent quality selection, the number of aGUVs considered of the highest quality was still limited. The use of 1 mM Mg^{2+} as the initiator yielded not only the best results in terms of the aGUV quality and yield, it also provides the additional benefit of enabling studies aimed at investigating the interaction of Ca^{2+} with PI(4,5)P_2 without releasing unphysiologically high levels of Mg^{2+} from the EDTA upon the addition of Ca^{2+}. Compared to an earlier study aimed at fabricating PS containing aGUVs,[31] obtaining PI(4,5)P_2 containing sGUVs and aGUVs in physiological salt conditions turns out to be significantly more challenging. Overall, however, this study has shown that PI(4,5)P_2 containing aGUVs can be obtained, which will provide the foundation for future studies aimed at studying lipid raft/PI(4,5)P_2

domain interactions. Expanding the work to other PIPs or anionic lipids will require in all likelihood careful adjustments to the experimental conditions.

Data availability

Original data are available at **https://asymvesiclepip2.wpi.edu/**

Author contributions

TAP, AHR and AG were responsible for conceptualization, methodology, writing (original draft and review), TAP was additionally responsible for the investigation, validation and formal data analysis. AG, AHR supervised the project and acquired funding.

Conflicts of interest

The authors report no conflict of interest.

Note added in proof

Fig. 6 was revised following a question from Dr Thais Enoki, see DOI: **10.1039/D5FD90019K**.

Acknowledgements

This work was funded by the National Science Foundation CHE-1904886.

References

1 Y. Wen, V. M. Vogt and G. W. Feigenson, *Annu. Rev. Biochem.*, 2021, **90**, 681–707.
2 Y. Wen, G. W. Feigenson, V. M. Vogt and R. A. Dick, *J. Mol. Biol.*, 2020, **432**, 5343–5364.
3 X. Li, Y. Miao, D. S. Pal and P. N. Devreotes, *Semin. Cell Dev. Biol.*, 2020, **100**, 133–142.
4 M. P. Krahn, *Front. Cell Dev. Biol.*, 2020, **8**, 277.
5 M. G. Waugh, S. Minogue, D. Chotai, F. Berditchevski and J. J. Hsuan, *J. Biol. Chem.*, 2006, **281**, 3757–3763.
6 R. M. Adam, N. K. Mukhopadhyay, J. Kim, D. Di Vizio, B. Cinar, K. Boucher, K. R. Solomon and M. R. Freeman, *Cancer Res.*, 2007, **67**, 6238–6246.
7 A. Arcaro, M. Aubert, M. E. Espinosa del Hierro, U. K. Khanzada, S. Angelidou, T. D. Tetley, A. G. Bittermann, M. C. Frame and M. J. Seckl, *Cell Signal*, 2007, **19**, 1081–1092.
8 B. Cinar, N. K. Mukhopadhyay, G. Meng and M. R. Freeman, *J. Biol. Chem.*, 2007, **282**, 29584–29593.
9 C. M. Johnson, G. R. Chichili and W. Rodgers, *J. Biol. Chem.*, 2008, **283**, 29920–29928.
10 S. Das, S. Chakraborty and A. Basu, *J. Neurochem.*, 2010, **115**, 537–549.

11 F. Furt, S. Konig, J. J. Bessoule, F. Sargueil, R. Zallot, T. Stanislas, E. Noirot, J. Lherminier, F. Simon-Plas, I. Heilmann and S. Mongrand, *Plant Physiol.*, 2010, **152**, 2173–2187.
12 X. Gao, P. R. Lowry, X. Zhou, C. Depry, Z. Wei, G. W. Wong and J. Zhang, *Proc. Natl. Acad. Sci. U. S. A.*, 2011, **108**, 14509–14514.
13 L. Zhang, J. Li, P. Zhang, Z. Gao, Y. Zhao, X. Qiao and C. Chen, *Biophys. Rep.*, 2018, **4**, 25–38.
14 O. Cizmecioglu, J. Ni, S. Xie, J. J. Zhao and T. M. Roberts, *eLife*, 2016, **5**, e17635.
15 J. van Rheenen, E. M. Achame, H. Janssen, J. Calafat and K. Jalink, *EMBO J.*, 2005, **24**, 1664–1673.
16 I. Parmryd, J. Adler, R. Patel and A. I. Magee, *Exp. Cell Res.*, 2003, **285**, 27–38.
17 J. Myeong, C. G. Park, B. C. Suh and B. Hille, *Proc. Natl. Acad. Sci. U. S. A.*, 2021, **118**, e2025343118.
18 Y. Nagatsuka and Y. Hirabayashi, *Biochim. Biophys. Acta*, 2008, **1780**, 405–409.
19 A. S. Klymchenko and R. Kreder, *Chem. Biol.*, 2014, **21**, 97–113.
20 I. Levental, D. A. Christian, Y. H. Wang, J. J. Madara, D. E. Discher and P. A. Janmey, *Biochemistry*, 2009, **48**, 8241–8248.
21 Z. Jiang, R. E. Redfern, Y. Isler, A. H. Ross and A. Gericke, *Chem. Phys. Lipids*, 2014, **182**, 52–61.
22 Y. Wen, V. M. Vogt and G. W. Feigenson, *Biophys. J.*, 2018, **114**, 2630–2639.
23 T. A. Paratore, G. E. Schmidt, A. H. Ross and A. Gericke, *Chem. Phys. Lipids*, 2024, **264**, 105424.
24 H. T. Cheng, Megha and E. London, *J. Biol. Chem.*, 2009, **284**, 6079–6092.
25 H. T. Cheng and E. London, *Biophys. J.*, 2011, **100**, 2671–2678.
26 S. Chiantia, P. Schwille, A. S. Klymchenko and E. London, *Biophys. J.*, 2011, **100**, L1–L3.
27 F. A. Heberle, D. Marquardt, M. Doktorova, B. Geier, R. F. Standaert, P. Heftberger, B. Kollmitzer, J. D. Nickels, R. A. Dick, G. W. Feigenson, J. Katsaras, E. London and G. Pabst, *Langmuir*, 2016, **32**, 5195–5200.
28 M. Son and E. London, *J. Lipid Res.*, 2013, **54**, 3385–3393.
29 T. A. Enoki and G. W. Feigenson, *Biophys. J.*, 2019, **117**, 1037–1050.
30 T. A. Enoki and G. W. Feigenson, *Biochim. Biophys. Acta, Biomembr.*, 2022, **1864**, 183995.
31 J. McDonough, T. A. Paratore, H. M. Ketelhohn, B. C. DeCilio, A. H. Ross and A. Gericke, *Membranes*, 2024, **14**, 181.
32 T. A. Enoki, J. Wu, F. A. Heberle and G. W. Feigenson, *Biochim. Biophys. Acta, Biomembr.*, 2021, **1863**, 183586.
33 T. A. Enoki, J. Wu, F. A. Heberle and G. W. Feigenson, *Data Brief*, 2021, **35**, 106927.
34 E. E. Kooijman, K. E. King, M. Gangoda and A. Gericke, *Biochemistry*, 2009, **48**, 9360–9371.
35 Y. H. Wang, A. Collins, L. Guo, K. B. Smith-Dupont, F. Gai, T. Svitkina and P. A. Janmey, *J. Am. Chem. Soc.*, 2012, **134**, 3387–3395.
36 K. Han, A. Gericke and R. W. Pastor, *J. Phys. Chem. B*, 2020, **124**, 1183–1196.
37 K. Han, S. H. Kim, R. M. Venable and R. W. Pastor, *Proc. Natl. Acad. Sci. U. S. A.*, 2022, **119**, e2202647119.
38 T. Balla, *Physiol. Rev.*, 2013, **93**, 1019–1137.
39 J. O. De Craene, D. L. Bertazzi, S. Bar and S. Friant, *Int. J. Mol. Sci.*, 2017, **18**, 634.

40 Y. Posor, W. Jang and V. Haucke, *Nat. Rev. Mol. Cell Biol.*, 2022, **23**, 797–816.
41 V. S. Yerramilli, A. H. Ross, S. Scarlata and A. Gericke, *Biophys. J.*, 2022, **121**, 793–807.
42 T. E. Rusten and H. Stenmark, *Nat. Methods*, 2006, **3**, 251–258.
43 G. Rouser, S. Fkeischer and A. Yamamoto, *Lipids*, 1970, **5**, 494–496.
44 J. Pazzi and A. B. Subramaniam, *ACS Appl. Mater. Interfaces*, 2020, **12**, 56549–56561.
45 A. Cooper, V. Girish and A. B. Subramaniam, *Langmuir*, 2023, **39**, 5579–5590.
46 K. Carvalho, L. Ramos, C. Roy and C. Picart, *Biophys. J.*, 2008, **95**, 4348–4360.